3-D GPR Survey with a Modular System: Reducing Positioning Inaccuracies and Linear Noise

Lieven Verdonck and Frank Vermeulen
Department of Archaeology
Ghent University
Ghent, Belgium
Lieven.Verdonck@UGent.be

Abstract—**Recently, the use of ground-penetrating radar (GPR) arrays with a large number of antenna elements in a fixed configuration has become more common. The investment needed for these systems is significant. Although gradually expandable modular systems, consisting of antennas which can be used independently, do not match the fast acquisition of detailed datasets by means of multi-channel arrays, they can help finding a compromise between increased acquisition speed and (limited) resources. In modular systems, the separation between transmitter-receiver pairs is often larger than the sampling distance prescribed by the Nyquist theorem. As a consequence, additional profiles have to be recorded in between, which requires a high positioning precision. As a completely identical response for the different antennas in an array is difficult to achieve, stripes can occur in the horizontal slices, especially when ringing occurs. This complicates the interpretation of features in the direction of the survey lines. In this paper, a three-dimensional frequency-wavenumber filter is proposed, consisting in a combination of a circular filter and a fan filter. The application of this filter to GPR data collected at the Roman town Mariana (Corsica, France) showed a reduction of the stripe patterns, allowing a more reliable characterization of subtle archaeological structures.**

Keywords-3-D ground-penetrating radar; modular antenna array; ringing; 3-D frequency-wavenumber filtering; archaeological prospection

I. INTRODUCTION

In the last few years, the use of multi-channel ground-penetrating radar (GPR) systems has become more common. Also in archaeology, field tests have been conducted with stepped frequency continuous wave and pulsed antenna arrays, enabling rapid data collection over large areas at sampling intervals approaching the Nyquist sampling theorem [1],[2]. Most of these arrays consist of antennas fixed in a large frame, arranged so that the cross-line spacing is smaller than the physical size of the antenna. For example, each receiver antenna can be made to record signals of two adjacent transmitter antennas [1],[3], or the transmitter-receiver combinations are rotated 45° with respect to the survey direction [4]. Modular systems, where each single antenna can be used independently, do not equal the combined acquisition speed and dense sampling of multi-channel GPR systems. However, when the available resources do not allow the high levels of investment demanded by large multi-channel systems, survey speed can be increased by gradually expanding a modular system while spreading investment over time. Furthermore, large multi-channel arrays can be difficult to operate in restricted spaces and on sites with a rough surface or otherwise inaccessible for systems towed behind a vehicle. As a consequence, it would be necessary to have a maneuverable single-channel instrument at one's disposal, as well as a multi-channel system [5]. Modular systems can be a solution when surveys often have to be carried out in difficult environments. This paper presents a full-resolution 3-D survey with a pulsed modular GPR system, conducted at the Roman town Mariana in Corsica (France). The required positioning precision is discussed and three-dimensional frequency-wavenumber (*f-k*) filtering is applied to suppress stripes along the survey lines, which can be a consequence of using multi-antenna systems.

II. DATA ACQUISITION AND POSITIONING

An area of 85 by 35 m was surveyed in October 2010 with a Sensors & Software Spidar network consisting of three pulseEKKO PRO 500 MHz antennas. A single antenna casing is approximately 0.23 m wide. The antennas were fixed onto a wheeled frame towed behind an all-terrain vehicle (ATV), so that the distance between the antenna midpoints was 0.25 m (Fig. 1).

Figure 1. Three antennas fixed onto a frame towed behind an ATV, with a distance between the antenna midpoints of 0.25 m. The total station prism is mounted as lowly as possible above the center of the middle antenna, to minimize errors due to uneven topography. An odometer wheel triggers the system every 0.05 m.

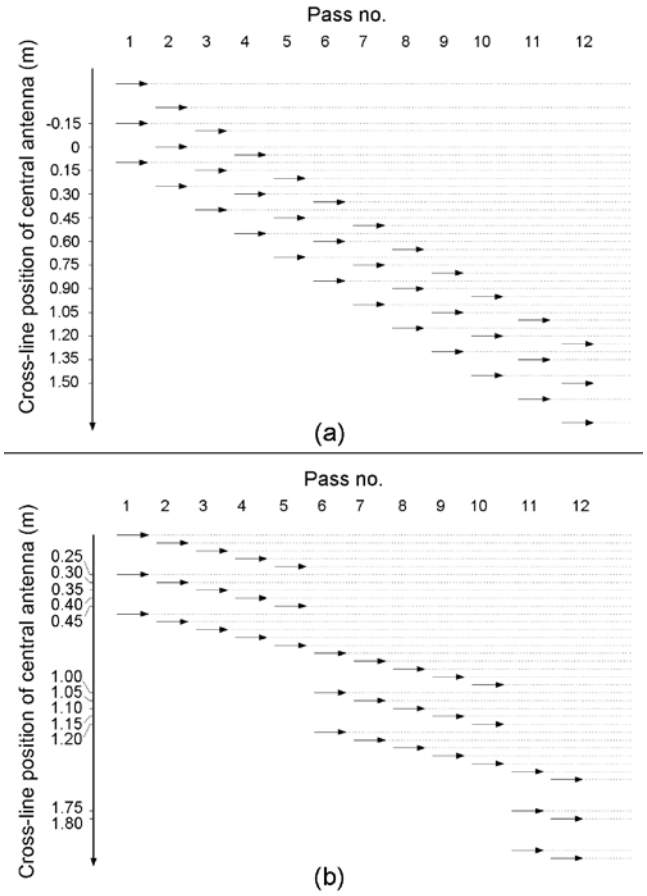

Figure 2. Two possible data recording schemes for a GPR system consisting of three antennas with a separation between the antenna midpoints of 0.25 m and a desired transect spacing of 0.05 m. For clarity, a different starting point has been given to each pass. In scheme (a) all passes are separated by 0.15 m. In scheme (b) five consecutive passes are 0.05 m apart, followed by an interval of 0.55 m.

To perform a full-resolution 3-D survey, a transect spacing of not more than quarter wavelength is required. For this survey this means a profile spacing of 0.05 m given an average subsurface velocity of *c*. 0.1 m/ns. As a result, the antennas were at a distance equal to five times the desired transect spacing. To obtain a 0.05 m separation, two schemes were tried out (Fig. 2). In the first scheme, all passes were separated by 0.15 m. In the second one, five consecutive passes were 0.05 m apart, followed by an interval of 0.55 m. Although both schemes yielded the same data quality, the second one is preferable, as the recording of the first and the last passes of the survey can happen more efficiently and the sorting of the profiles is less complicated. Along the transects, a measurement was triggered every 0.05 m by an odometer wheel. The stack was 8, the temporal sampling interval was 0.2 ns, and the time window was 60 ns.

For the positioning, a tracking total station (terrestrial positioning system, TPS) was used. In order to unambiguously assign each GPR measurement to the correct quarter wavelength grid position, coordinate precision should be better than one eighth of a wavelength [6]. For the survey presented here, this equals 0.025 m. When assessing the capability of a positioning instrument to fulfill this requirement, the accuracy for static and dynamic measurements is important. Furthermore, latency and synchronization errors between distance and angle measurements have to be considered.

For the instrument used (a Leica TCRP1201+), standard distance measurements in static mode have an accuracy of 1 mm + 1.5 ppm, and angle measurements are accurate to within 0.3 mgon, according to the technical data provided by the manufacturer [7]. These values are not applicable when the TPS is tracking a prism mounted above a moving GPR antenna (Fig. 1). For combined kinematic GPR-TPS measurements, the instrument specifications (for the TCRP1201+ in tracking mode a distance measurement accuracy of 3 mm +1.5 ppm is given) do not provide the full picture. The signal is processed within the TPS base station and is transferred to the remote control on the ATV (for this survey a CS15 controller was used) via built-in radio modems. Subsequently, it is sent to the GPR control unit via a serial cable, where it is fused with the most recent GPR trace. These different steps cause a time delay between the position measurement and the availability of the measurement, often referred to as latency. Recently, a method for the estimation of latency was presented [8]. Forward and reverse GPR profiles over targets generating strong diffractions (metal pipes) were compared by means of correlation and other fidelity measures, after spatially relocating the GPR traces using a range of latency correction times. Latency showed no temporal variations and was found to be independent on acquisition speed.

Beside a wrong inline position of GPR traces caused by latency, crossline deviations from the predefined transects can arise when using the TPS in tracking mode [9]. In order to estimate possible orthogonal deviations in our survey data, the TPS prism was mounted above a single GPR antenna which was towed manually between two parallel 90 m long guidance ropes, 0.25 m apart and laid out carefully so that the prism would follow a calibration line with coordinate y = 50 m as closely as possible. The TPS was at a position with coordinates x = 45 m and y = 0 m. First the GPR antenna with TPS prism was moved very slowly along the calibration line in order to assess its linearity, which resulted in measurements with an average y-coordinate of 49.996 m and a standard deviation of 0.009 m. Subsequently, tests with higher speed (from ~0.5 to ~1.5 m/s) were conducted. These yielded systematic errors in the y-coordinates exceeding 0.05 m near the extremities of the calibration line when the antenna was moved faster than 1 m/s (thus considerably exceeding the 1/8 wavelength criterion), and a symmetric pattern for forward and reverse profiles became apparent (Fig. 2a-b).

These crossline coordinate errors occur when distance and angle measurements are not achieved simultaneously [10], as is illustrated in Fig. 2c, a representation of a measuring sequence in a three-dimensional, Cartesian coordinate system $S(x, y, z)$ where the TPS is at position P_{TPS}. The distance measurement is made when the target is at position P_{dist}. Because of the time delay

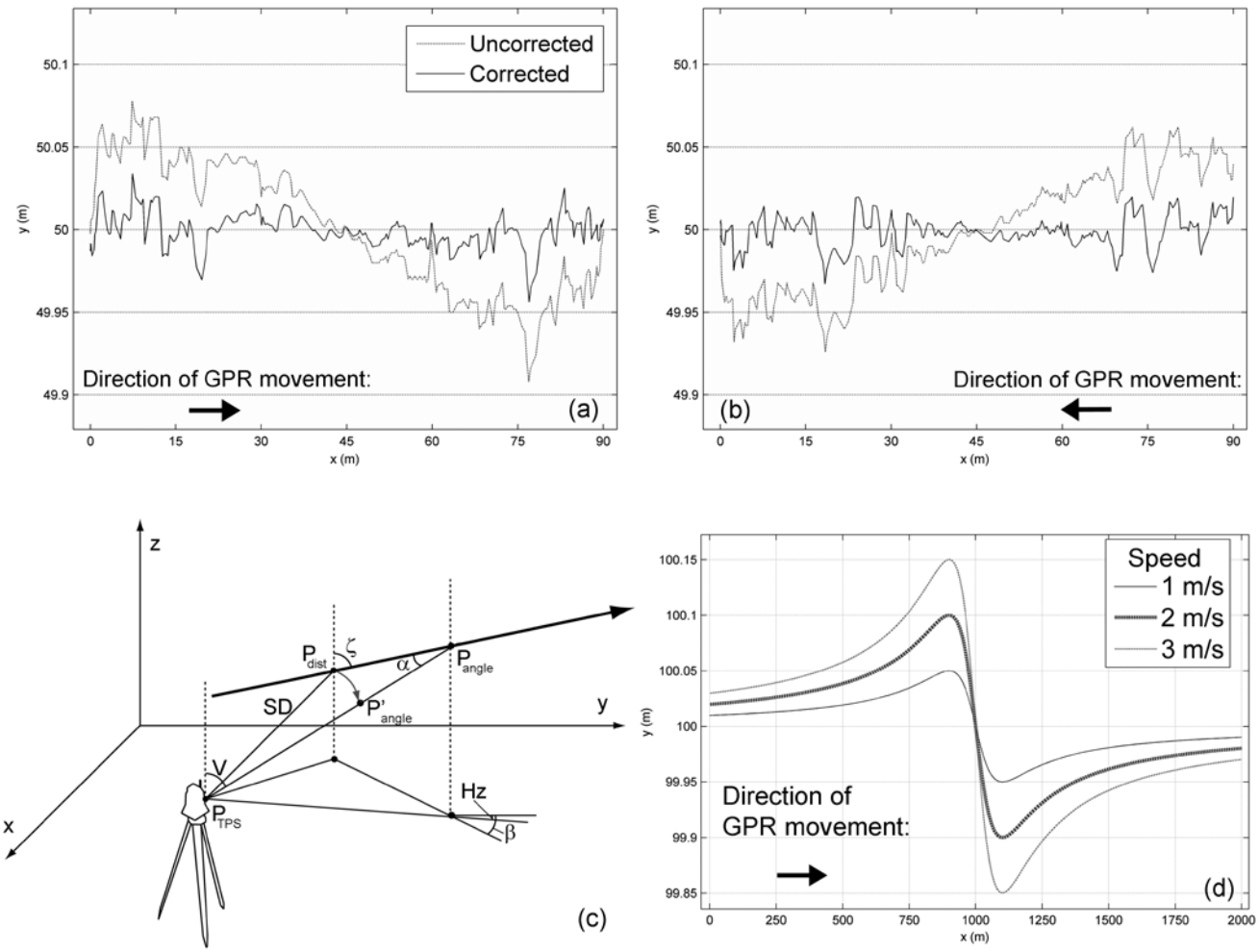

Figure 3. Fig. 3. (a-b) Dynamic positioning inaccuracies observed when moving along a calibration line with coordinates 0 m $\leq x \leq$ 90 m and y = 50 m, at an average speed of ~1.15 m/s, caused by bad synchronization of TPS distance and angle measurements. The corrected coordinates are also shown. The TPS was located at x = 45 m and y = 0 m. (c) Because of this time delay, the recorded position of the target is P'_{angle}, whereas in reality its position is P_{angle}. The resulting error is largest when α approaches 0° or 180°, it is minimal when α = 90°. The orthogonal deviation from the predefined line is maximal when α = 45° or 135°. For the explanation of the other symbols, please refer to the text. Illustration after [10], with modifications. (d) Simulation of the coordinates recorded by a tracking TPS at position x = 1000 m and y = 0 m, of a target moving along a line with coordinates 0 m $\leq x \leq$ 2000 m and y = 100 m. The TPS has synchronization error Δt = 0.1 s. Positioning accuracy decreases as the target speed increases.

$$\Delta t = t_{angle} - t_{dist}, \quad (1)$$

where t_{angle} is the time of the angle measurement and t_{dist} is the time of the distance measurement, the position of the target recorded by the TPS is $P'_{angle}(x'_{angle},y'_{angle},z'_{angle})$, whereas the real position of the target at t_{angle} is $P_{angle}(x_{angle},y_{angle},z_{angle})$. Using the slope distance (SD), the horizontal angle (Hz) and the vertical angle (V) resulting from the TPS measurement, the true position P_{angle} is given by [10]:

$$x_{angle} = x'_{angle} + v\,\Delta t\,[\cos\alpha - 1/2\,(v\,\Delta t / SD)\,(1 - \cos^2\alpha)]\,\sin V \sin Hz, \quad (2)$$

$$y_{angle} = y'_{angle} + v\,\Delta t\,[\cos\alpha - 1/2\,(v\,\Delta t / SD)\,(1 - \cos^2\alpha)]\,\sin V \cos Hz, \quad (3)$$

$$z_{angle} = z'_{angle} + v\,\Delta t\,[\cos\alpha - 1/2\,(v\,\Delta t / SD)\,(1 - \cos^2\alpha)]\,\cos V, \quad (4)$$

where

$$\cos\alpha = \cos\zeta \cos V + \sin\zeta \sin V \cos(\beta - Hz). \quad (5)$$

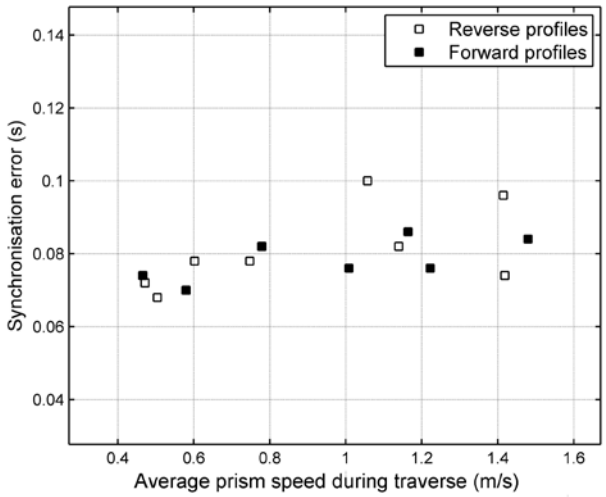

Figure 4. In order to correct the data collected along the calibration line (Fig. 3a-b), for each traverse a range of Δt values were evaluated using (2)-(4) in the text. The value yielding the coordinate series with the lowest standard deviation around the predefined line with y-coordinate = 50 m was considered the optimum value. From these tests a mean synchronization error of 0.080 s emerged, with a standard deviation of 0.009 s.

The speed of the moving target v was estimated by looking at the two nearest points surrounding $P'_{angle,i}$ ($P'_{angle,i-1}$ and $P'_{angle,i+1}$) and the two nearest observation times around $t_{angle,i}$ ($t_{angle,i-1}$ and $t_{angle,i+1}$), so that:

$$v = [\,(x'_{angle,i+1} - x'_{angle,i-1})^2 + (y'_{angle,i+1} - y'_{angle,i-1})^2 + (z'_{angle,i+1} - z'_{angle,i-1})^2\,]^{1/2} / (t_{angle,i+1} - t_{angle,i-1}), \quad (6)$$

and β was approximated by:

$$\tan\beta = (x'_{angle,i+1} - x'_{angle,i-1}) / (y'_{angle,i+1} - y'_{angle,i-1}). \quad (7)$$

The position of the TPS in relation to the direction of the prism movement (which coincides with the direction of the GPR profile) affects the magnitude of the positioning error and its inline and crossline components. The positioning error is maximal when the angle α between the line of sight P_{TPS} - P_{angle} and the prism movement approaches 0°. Its magnitude is then obtained from (3), for V = 90° and $Hz = \alpha = 0°$, and equals $v\Delta t$. In that case, only an x-coordinate error and no y-coordinate error exists (leaving aside possible z-coordinate errors). This is also visible in Fig. 2d, which simulates the coordinates of a target moving along a line with y-coordinate = 100, measured by a TPS with a synchronization error Δt = 0.1 s, at a position with coordinates x = 1000 and y = 0. The positioning error approaches 0 when α = 90°, i.e. when the line of sight is perpendicular to the movement of the GPR. At angles α = 45° or 135°, it equals $v\Delta t$ ($\sqrt{2}$)/2. In this case the theoretical y-coordinate error is maximal (0.5 $v\Delta t$), and equals the x-coordinate error.

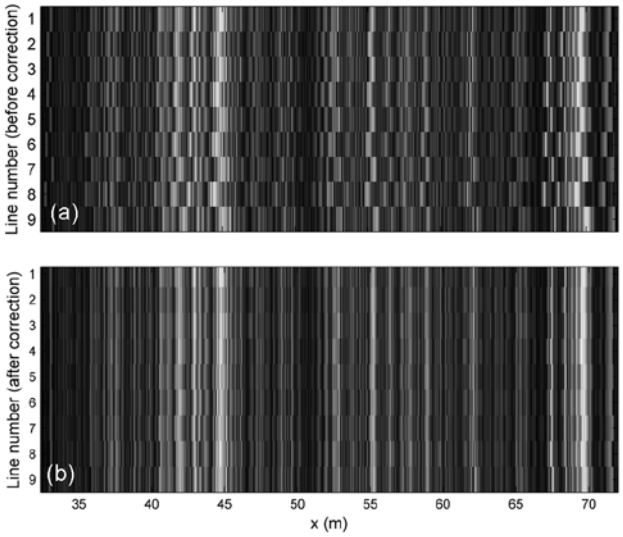

Figure 5. Squared GPR amplitude, averaged over two-way travel times between 10 and 11 ns, originating from 9 profiles over several roman structures. Each profile had the same coordinates (0 m $\leq x \leq$ 90 m, y = 50 m; see Fig. 3a-b), but the GPR towing speed was higher for increasing profile number (from ~0.5 m/s up to 1.5 m/s). The TPS was at a position with coordinates x = 45 and y = 0. Odd-numbered lines were recorded in reverse direction, even-numbered lines in forward direction. (a) Results before correction of synchronization error and latency. The x-coordinate discrepancies become larger as the prism speed is higher. (b) The same data, after correction of a synchronization error of 0.08 s and a latency of 0.13 s.

The above equations were applied for the correction of the data collected along the calibration line (Fig. 2a-b). For each traverse, a range of values for Δt between 0 and 0.25 s, with a step of 0.002 s were evaluated. The Δt value yielding the corrected coordinate series with the lowest standard deviation around coordinate y = 50 m was considered the optimum value. Fig. 4 shows the optimum values for the different traverses as a function of the average prism speed during the traverse. From these tests a mean synchronization error Δt of ~0.080 s emerged, with a standard deviation of 0.009 s. Although a precise determination of the synchronization error can only happen by means of calibration lines in the laboratory or in combination with accurate GPS measurements, and although it has been demonstrated that Δt shows periodical variations [10], a good approximation can be found using a simple field test as described above. Using the synchronization error of 0.080 s, it was possible to correct the deviations in the y-coordinates so that these rarely exceed 0.025 m. For example, for the traverse shown in Fig. 2a, the standard deviation decreased from 0.042 m (uncorrected) to 0.021 m (after correction).

If the synchronization error Δt is constant, the positioning accuracy decreases as the speed of the moving prism increases (Fig. 2d). Whereas the x-coordinate errors can be eliminated through a latency correction as mentioned above, this is not the true for the y-coordinate inaccuracies, which can deteriorate the data quality, especially from 3-D surveys. Some modern TPS instruments have a built-in synchronization tool, but this is not always the case. For example, for the Leica TPS 1200+, synchronisation is available in tracking mode when operated from the RX1250 remote control running the Smartworx

software, but not from the CS15 controller running the Smartworx Viva software (which was used for the survey presented in this paper).

After correcting the synchronization error, an inline mismatch remained between GPR profiles recorded in forward and reverse direction along the calibration line. These *x*-coordinate errors were estimated by applying latency corrections between 0 and 0.25 s with steps of 0.002 s, as described in [8], and the match of the latency corrected profile pairs was quantified using cross-correlation. This resulted in a mean latency of 0.130 s, with a standard deviation of 0.008 s. Fig. 5 illustrates the effect of synchronization error and latency corrections on the *x*-coordinate accuracy. From repeats of the same GPR profile, recorded with increasing towing speed (from ~0.5 m/s up to ~1.5 m/s), the squared amplitude was averaged over two-way travel times between 10 and 11 ns. The trace spacing along the profiles was 0.025 m. As speed increased, the discrepancies between the *x*-coordinates of GPR features in forward and reverse lines became larger (Fig. 5a). After correction of a synchronization error of 0.08 s and a latency of 0.13 s, traces are correctly repositioned (Fig. 5b).

Apart from the static and dynamic positioning accuracy of the total station itself, coordinate precision also implies that the quarter wavelength transect line has to be followed precisely with the GPR during data acquisition. For the survey presented here, both errors together should not be larger than 0.025 m. When using a wide array with fixed, closely spaced antennas, the whole survey area is densely sampled provided that swaths are parallel and slightly overlapping [1]. In the case of an array with a distance between the 500 MHz antennas of 20 cm or more, additional profiles have to be recorded in between (Fig. 2). Coordinate precision then becomes very important for an efficient data collection which at the same time respects the quarter wavelength criterion. During the field tests, maintaining the necessary precision proved difficult without guide ropes, even when the ATV was driven very slowly and when a guidance system was utilized. A different procedure consisted in putting small stakes along tape measures laid out in cross-line direction over the survey area every 40 m, and moving the stakes for every pass. When keeping the stakes perfectly in line, it was possible to follow the theoretical grid line to within 0.02 m.

The driving speed was around 1 m/s, although with the same settings higher speeds were possible (up to 2 m/s). It took 13 hours for two people to record 234 passes of 85 m length, which were all in the same (eastern) direction. This acquisition speed was approximately the same as for previously conducted single antenna surveys in zigzag mode, although for the modular system with three antennas, the profile length acquired in a given amount of time was three times higher than for the single-antenna surveys.

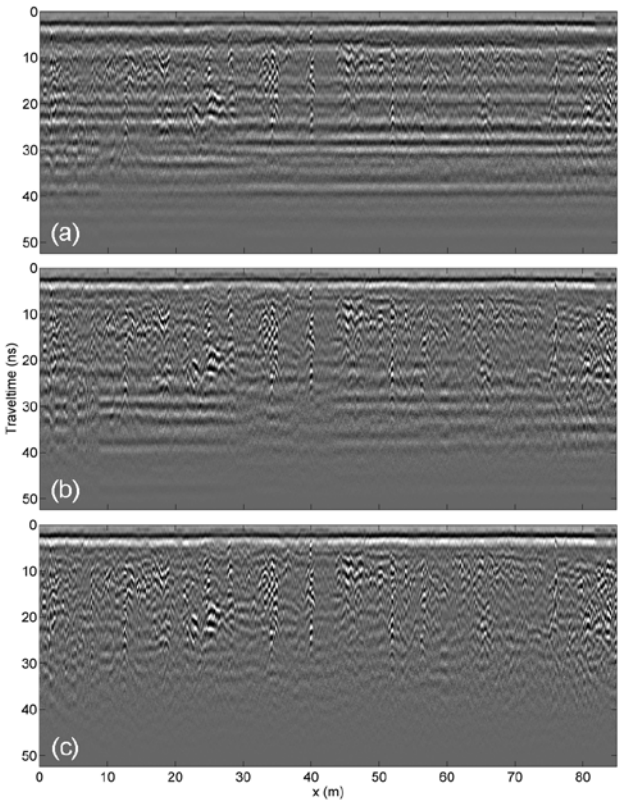

Figure 6. GPR profile showing ringing noise. (a) Raw data. (b) The same profile after background removal. (c) The same profile after application of a combined fan filter and circular filter in the three-dimensional *f-k* domain.

III. DATA PREPROCESSING

First of all, the corrected horizontal coordinates were assigned to the GPR traces recorded by the central antenna, over which the total station prism was mounted (Fig. 1). Because the total station allowed a coordinate acquisition with a frequency of 5 Hz, position data were not available for every GPR trace. To the intermediate traces, coordinates were assigned by spline interpolation between the two nearest available total station measurements. The coordinates of the two side antennas were calculated taking into account the direction of the central antenna, which was determined by looking at the two nearest surrounding coordinates. Using the angle between this direction and the theoretical transect, and the known offset of the side antennas (0.25 m), their *x*- and *y*-coordinates were defined. After dewow (using a window of 4 ns), an average trace was calculated for each transect. Of these average traces, the first negative troughs following the start of the air-wave were aligned. This occurred by searching the minimum of the samples in a 2 ns window around an initial value, visually determined on a plot with all juxtaposed average traces. The data were then interpolated onto a regular grid of 0.05 x 0.05 m using Delaunay triangulation, involving linear interpolation between the amplitudes at the corners of the surrounding triangle. Subsequently, the same gain function was applied to all traces to enhance later arrivals. It was based on the inverse average envelope of the amplitude of all traces,

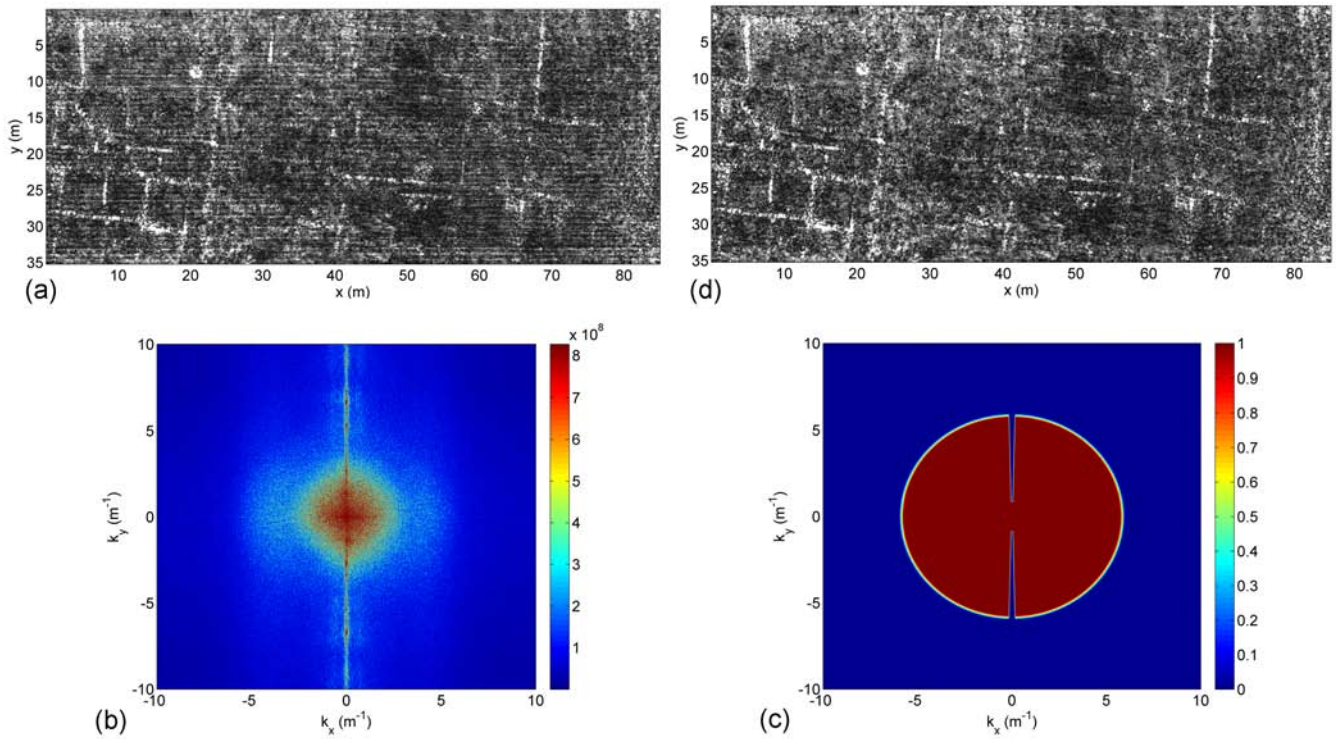

Figure 7. (a) Frequency slice (332 MHz) showing a striped pattern because of ringing which affects the antennas differently. (b) Frequency-horizontal wavenumber spectrum of the slice in (a). (c) Combination of fan filter and circular filter to attenuate the stripe pattern. (d) Slice (a) after application of the filter.

and smoothed using a moving average filter with a length of 15 samples (3 ns).

IV. Reducing Linear Noise

In the profiles, considerable horizontal and subhorizontal banding was visible (Fig. 6a). Since the Spidar network has been designed so that only one transmitter can be active in a given receiver time window [11], it can be assumed that the noise is not caused by the direct wave generated by a transmitter belonging to a different antenna pair. Moreover, nearly identical noise patterns were observed during previous surveys with a single-channel system. As a GPR antenna is located on the ground, its impedance is strongly influenced by the ground. On certain soils (e.g. clay-rich or wet soils) this may produce a mismatch between the antenna and the feed cable, causing the currents to bounce between the feed and the ends of the antenna. Consequently, the transmitter antenna transmits several pulses decaying with time instead of a single pulse, although this residual response, often referred to as system ringing, can also occur on the receiver [12]. During our survey, this effect was also influenced by the position of the antenna cable, since it was observed that the pattern of the horizontal bands changed as the cable was slightly moved, and although it was made sure that the cable did not touch the antenna housing. The presence of a cable in the vicinity of the GPR can act as a source of radiation and generate or enhance ringing [13]. Although the antennas are tuned in order to show as similar responses as possible [11], the ringing was slightly different in transects recorded with different antennas, which provoked stripes in the horizontal slices, along the survey lines (Figs. 7a and 8a). In circumstances without ringing (e.g. on sandy soils as compared to sandy loam for the site presented here) no differences in amplitude were noticeable between the different antennas.

A. *Filtering techniques*

Several techniques have been proposed to remove ringing noise. The simplest way is to subtract the average of all traces in a profile from each individual trace (background removal). This method only partially removed the ringing from the data collected at Mariana, because often the amplitude of the banding strongly varies along the profile and since it is not always perfectly horizontal (Fig. 6b, see also the horizontal slice in Fig. 8b). Other approaches include spectral whitening followed by energy matching (calculating the energy for each profile at a certain time or depth, and matching the resulting values) [14], frequency-wavenumber (*f-k*) filtering, Radon transform, discrete wavelet transform and eigenimage filtering using singular value decomposition [15]. Although it has been shown that advanced methods like discrete wavelet transform and Radon transform are in certain cases superior to *f-k* techniques [16], a three-dimensional *f-k* filter applied to a full-resolution GPR dataset can be efficient in separating system ringing noise from the desired features with minimal distortions of the signal, as is shown below.

B. *Combination of a circular filter and a directional filter in the f-kx-ky domain*

In the Mariana dataset, the linear banding in the direction of the survey lines (i.e. in the *x*-direction, Fig. 7a) in the frequency-horizontal wavenumber (f-k_x-k_y) domain could be expected to be concentrated along the k_y axis. For the higher frequencies (above 400 MHz) it was concentrated in a narrow band along the whole k_y axis (Fig. 7b), and was isolated by a filter suppressing k_x values from -0.05 to 0.05 m^{-1}. For the lower frequencies, in general the signal to noise ratio was lower, and on the frequency slices, shorter stripes which do not span the whole length of the survey area showed more clearly. In the f-k_x-k_y domain, these have a higher k_x value, hence the noise was visible as a wider band along the k_y axis. This resulted in a larger overlap with the desired reflections from archaeological structures, e.g. long wall portions in the *x*-direction, especially in areas with lower k_y values (the width of the walls varies between 0.3 and 0.6 m). There it was impossible to fully separate the striping effect from the signal and filtering was conservative, i.e. the noise was not filtered in its entire bandwidth. After a number of trial coefficients had been applied, the best results were obtained using a fan filter, broadening towards the extremities of the k_y axis (Fig. 7c) and for decreasing frequencies. Near the extremities, the noise region was filtered in its entire width (i.e. k_x values from -1.25 to 1.25 m^{-1} were suppressed for the lowest frequencies). An area near the centre with radius 1 m^{-1} (decreasing to 0.5 m^{-1} for the lowest frequencies), was excluded from any filtering. It contains the slowly varying part of the data (geological or pedological background) which does not contribute to the noise stripes. Although the contribution of the striping effect in the f-k_x-k_y domain is concentrated along the k_y axis, it is not restricted to that area. For the higher frequencies, the stripes mainly consist of noise with a high wavenumber. Although here too it was not possible to completely separate the noise from the signal, the result of the filtering was improved by combining the fan filter with a circular low-pass filter, with a uniform radius of 6 m^{-1} for all frequencies. Again this was the result of applying different filter sizes and evaluating the outcome. The result of applying the combined fan filter and circular filter is shown in Figs. 6c, 7d and 8c. The images contain significantly less noise lines.

Further data processing included the application of elevation static corrections. In order to obtain a planar surface, a plane was fitted to the slightly undulating survey area, minimizing the root mean square error [17]. The maximal difference in elevation between the survey area and the plane was 0.34 m, although these maximum values only occurred near the extremities of the prospection zone. Height differences for the large central part of the surface were not bigger than 0.15 m. Subsurface velocity was estimated by applying a 2-D Stolt migration algorithm on single GPR profiles, using a range of constant velocities. The velocity was found to decrease from 0.11 m/ns for the shallow layers to approximately 0.08 m/ns at a depth of 1 m. The data were then 3-D phase shift migrated using the obtained velocity function, which was also used for the time-to-depth conversion.

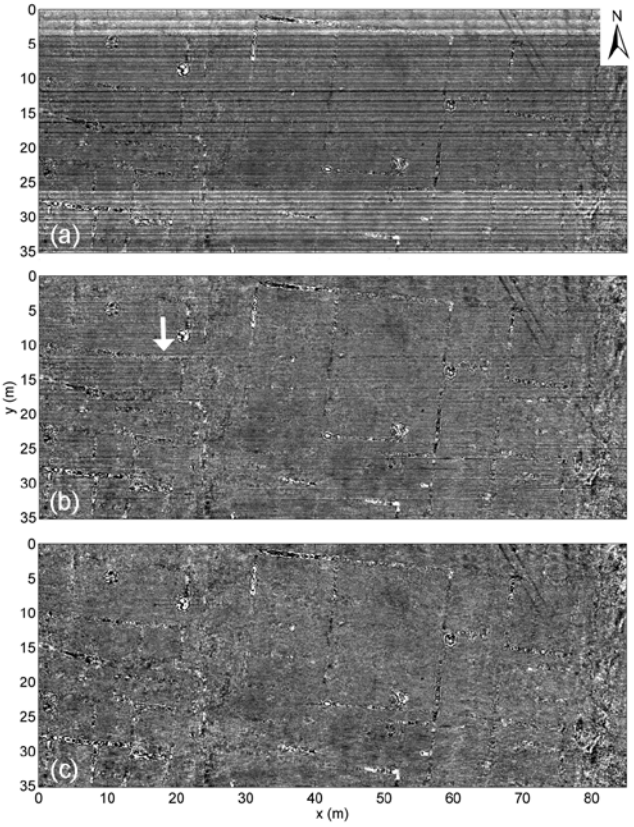

Figure 8. Especially in the deeper horizontal slices, noise lines can pose a problem for the interpretation of subtle archaeological features. (a) Raw horizontal slice at a depth of approximately 1 m. Except for the northern part (between 0 and 4.5 m), the survey was carried out following the recording scheme in Fig. 2b. Therefore each time five profiles recorded with the same antenna lay side by side, resulting in 0.25 m wide noise stripes. (b) The same slice after background removal. The wall structure near the arrow is still obscured by linear noise. (c) The same slice, after application of f-k filtering but before migration. The extent of the wall can now more easily be defined.

V. RESULTS

The 3-D survey carried out in 2010 (Fig. 9) fits into the archaeological picture known from excavations and earlier geophysical surveys [18]. Two *c.* 9.5 m wide, parallel streets are visible (Fig. 9, nos. 1 and 2), with the same orientation as observed in the rest of the town. The space between the two streets is largely taken up by a building consisting of a series of rooms around a courtyard (Fig. 9, no. 3). This can probably be interpreted as a large *domus* (house). In one of the rooms a floor can be distinguished (no. 4). One of the buildings in the western part of the survey area can equally be recognized as a house. Underneath its entrance, a drain or channel runs towards the street (no. 5). In several locations, there are indications for later alterations (e.g. nos. 6, 7 and 8). Most walls share the same orientation, exceptions are nos. 9 and 10.

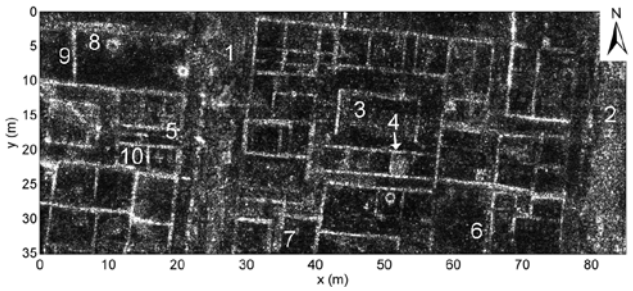

Figure 9. 3-D migrated horizontal slice at an approximate depth of 0.72-0.75 m, showing a large Roman house (3) between two parallel streets (1 and 2). One of the rooms shows a floor (4). Underneath the entrance of a second, smaller house, a drain runs towards the street (5). At several locations there are indications for structural alterations (6-8). A few walls show a slightly different alignment (9 and 10).

VI. Conclusions

The advent of multi-channel GPR systems with a large number of fixed, closely spaced antennas has enabled large scale high-resolution surveys while drastically reducing the recording time in the field. Modular, gradually expandable systems consisting of conventional single-channel instruments do not equal these high-performing systems when it comes to combined acquisition speed and sampling density. On the other hand, the level of investment is less demanding and can be spread in time. When a modular system consists of a small number of antennas, recording schemes are complex. As the transect spacing is larger than the required profile separation for a 3-D survey, additional passes are necessary to record the profiles in between. Consequently, positioning accuracy and precision are crucial. For TPS instruments, beside instrument accuracy in static and dynamic mode, latency is important. A specific form of latency, the time delay between distance and angle measurement was described in detail in this paper. Furthermore, a critical factor is how close the theoretical grid line can be followed by the operator. Today it is still difficult to keep a vehicle-towed system close enough to the grid line so that the sum of instrument errors and operation error stays below the quarter wavelength sampling criterion, especially for surveys with higher frequency antennas. In the future, new guidance solutions may overcome this issue. Even if antennas have been tuned carefully, images from a multi-channel GPR can contain stripes in the direction of the survey lines, especially when the soil properties or the roughness of the surface result in ringing. The removal of these noise stripes is essential, as they may obscure subtle reflections in the direction of the transects. For the case study presented, three-dimensional *f-k* filtering using a combination of a circular filter and a fan filter proved effective, while distorting the signal only to a minimal extent.

Acknowledgments

The research leading to these results has received funding from the European Community's Seventh Framework Programme (FP7/2007-2013) under grant agreement n° 230679, under the action Marie Curie – People IAPP, with the Project entitled "Radiography of the past. Integrated non-destructive approaches to understand and valorise complex archaeological sites". The authors would like to thank C. Corsi, scientific coordinator Radio-Past project, the Direction Régionale des Affaires Culturelles de Corse and J. Cesari, Conservateur Régional de l'Archéologie for supporting this survey. The support of D. Istria, director of the Mariana project, the municipality of Lucciana and the Association Culturelle de Mariana et de la Basse Vallée du Golo during the fieldwork is gratefully acknowledged. We thank Sensors & Software Inc. for their advice on several topics discussed in this paper. This study would not have been possible without the support of the Fund for Scientific Research – Flanders and of the Special Research Fund of Ghent University.

References

[1] N. Linford, P. Linford, L. Martin, and A. Payne, "Stepped frequency ground-penetrating radar survey with a multi-element array antenna: results from field application on archaeological sites," Archaeol. Prospect., vol. 17, no. 3, pp. 187-198, 2010.

[2] J. Leckebusch, "Comparison of a stepped-frequency continuous wave and a pulsed GPR system," Archaeol. Prospect., vol. 18, no. 1, pp. 15-25, 2011.

[3] I. Trinks, B. Johansson, J. Gustafsson, J. Emilsson, J. Friborg, C. Gustafsson, J. Nissen, and A. Hinterleitner, "Efficient, large-scale archaeological prospection using a true three-dimensional ground-penetrating radar array system," Archaeol. Prospect., vol. 17, no. 3, pp. 175-186, 2010.

[4] R.G. Francese, E. Finzi, and G. Morelli, "3-D high-resolution multi-channel radar investigation of a Roman village in Northern Italy," J. Appl. Geophys., vol. 67, no. 1, pp. 44-51, 2009.

[5] E. Utsi, "GPR as an imaging device: some problems and possible solutions," 13th International Conference on Ground-Penetrating Radar (GPR), 2010, doi: 10.1109/ICGPR.2010.5550136.

[6] M. Grasmueck and D. Viggiano, "Integration of ground-penetrating radar and laser position sensors for real-time 3-D data fusion," IEEE T. Geosci. Remote, vol. 45, no. 1, pp. 130-137, 2007.

[7] Leica Geosystems, Leica TPS1200+ User Manual Version 6.0. Heerbrugg: Leica Geosystems, 2008.

[8] U. Böniger and J. Tronicke, "On the potential of kinematic GPR surveying using a self-tracking total station: evaluating system crosstalk and latency," IEEE T. Geosci. Remote, vol. 48, no. 10, pp. 3792-3798, 2010.

[9] F. Lehmann and A. Green, "Semiautomated georadar data acquisition in three dimensions," Geophysics, vol. 64, no. 3, pp. 719-731, 1999.

[10] W. Stempfhuber, K. Schnädelbach, and W. Maurer, "Genaue Positionierung von bewegten Objekten met zielverfolgenden Tachymetern," 13th International Course on Engineering Surveying, pp. 144-153, 2000.

[11] Sensors & Software Inc., personal communication.

[12] S.J. Radzevicius, E.D. Guy, and J.J. Daniels, "Pitfalls in GPR data interpretation: differentiating stratigraphy and buried objects from periodic antenna and target effects," Geophys. Res. Lett., vol. 27, no. 20, pp. 3393-3396, 2000.

[13] A.P. Annan and J.L. Davis, "Design and development of a digital ground penetrating radar system," in Ground Penetrating Radar, Geological Survey of Canada Paper 90-4, J.A. Pilon, Ed., Ottawa: Geological survey of Canada, 1992, pp. 15-23.

[14] J. Leckebusch, "Use of antenna arrays for GPR surveying in archaeology," Near Surface Geophysics, vol. 3, no. 2, pp. 111-115, 2005.

[15] J. Kim, S. Cho, and M. Yi, "Removal of ringing noise in GPR data by signal processing," Geosciences Journal, vol. 11, no. 1, pp. 75-81, 2007.

[16] L. Nuzzo and T. Quarta, "Improvement in GPR coherent noise attenuation using τ-p and wavelet transforms," Geophysics, vol. 69, no. 3, pp. 789-802, 2004.

[17] R. Streich and J. van der Kruk, “Three-dimensional multicomponent georadar imaging of sedimentary structures,” Near Surface Geophysics, vol. 4, no. 1, pp. 39-48, 2006.

[18] L. Verdonck and F. Vermeulen, “GPR survey at the Roman town of Mariana (Corsica),” in Mémoire du sol, espace des hommes, D. Marguerie and P. Lanos, Eds., Rennes: Presses Universitaires de Rennes, 2009, pp. 241-243.